

CFD SIMULATION OF A SPOUTED BED WITH A NON-POROUS DRAFT TUBE

A. ABBASZADEH¹, S.H. HOSSEINI²

¹. Islamic Azad university, Ilam branch, IRAN

². Department of Chemical Engineering, University of Sistan and Baluchestan, Zahedan 98164-161, IRAN

ABSTRACT

A multi-fluid Eulerian–Eulerian approach incorporating the kinetic theory of granular flow was used to simulate a spouted bed containing non-porous draft tube. Solid and gas velocity vector, gas flow rate in annulus and spout regions and longitudinal pressure distribution were evaluated. The gas flow rate in annulus was also investigated for the bed with porous draft tube. In addition, the effects of the entrainment height and the draft tube diameter were studied. Simulation indicates the formation of three regions namely, annulus, spout and fountain; similar to a conventional spouted bed. Current model predicts acceptable results in both spout and annulus regions. Simulation results indicate that the model can be employed for both mono size and multi size particles reasonably. This paper provides useful basis for further works on understanding gas–solid flow mechanism in spouted beds containing a non-porous draft tube.

NOMENCLATURE

M Total number of solids phases
 I_{gmi} Momentum transfer from fluid phase to m^{th} solids phase; N/m³
 J_m Collisional dissipation, m²/s³
 P Pressure, Pa
 S_{mij} solid phase stress, Pa
 \mathbf{u} velocity vector, m/s
 u_m averaged velocity of phase m , m/s
 U superficial gas velocity, m/s
 U_{ms} minimum superficial gas velocity for spouting, m/s
 X_{gm} mass weighted concentration ratio

Greek letters

β_{gm} coefficient for the interphase force between the fluid phase and solids phases, Kg/m³.s
 β_{km} coefficient for the interphase force between the solids phases; Kg/m³.s
 α_i Volume fraction of phase i , dimensionless
 η function of restitution coefficient, dimensionless
 η_i ratio between Lagrangian and particle relaxation time scales
 Θ granular temperature, m²/s²
 κ_m solid thermal conductivity, W/m K
 μ_m solid viscosity, kg/m s

Π_m granular temperature exchange term, kg/m s³

ρ density, kg/m³

τ_{gij} Fluid-phase stress tensor, Pa

τ_{mij} stress tensor of phase m , Pa

INTRODUCTION

Nowadays spouted beds are widely used in various physical operations such as drying, coating and granulation and chemical applications such as coal gasification, catalytic partial oxidation, catalytic oxidative coupling reactors. Conventional spouted bed in gas-solid systems is an effective means of contacting for gas and coarse particles such as Geldart D. The insertion of an axially positioned non-porous draft tube into the conventional spouted bed has superiority due to the stability and the flexibility. Applications of the spouted bed with a non-porous draft tube has been developed in wide variety of chemical processes including drying (Khoe and Van Brakel, 1983), coal gasification (Hatate et al., 1996), combustion (Konduri et al., 1995), pyrolysis of hydrocarbon (Stocker et al., 1989), pneumatic conveying (Ferreira and Freire, 1992), pharmaceuticals (Fukumori and Ichikawa, 1997) and mixing (Krambrock, 1976). The flow characteristics of a non-porous draft tube spouted bed and its applications have been reviewed (Hatate et al., 1997). Ishikura et al. (2003) compared three types of spouted bed including conventional spouted bed, spouted bed with non-porous and porous draft tube in several hydrodynamics terms. They showed that pressure drop for spouting with a draft tube is lower than the conventional spouted bed. This is an advantage in conserving energy. In addition, they showed minimum spouting velocity U_{ms} of spouted bed with a draft tube is much lower than the conventional type. They indicated that the lowest U_{ms} pertain to the spouted bed with a non-porous draft tube. Altzibar et al. (2008) used a conical spouted bed with non-porous, porous, and open-sided draft tubes for drying fine particles. They found that non-porous draft tube requires the lowest minimum spouting velocity due to the low solid circulation rate and to the fact that no gas percolates to the annulus. They observed that the pressure drops of the bed with a non-porous and porous draft tubes are similar, while the pressure drop of the bed with an open-side tube is much larger than those of others. They showed that the solid circulation rate and the drying efficiency of the open-sided draft tube are superior to any other spouted bed configuration. Spouted bed with a non-porous draft tube is not proper when the gas phase has an active role such as drying and reaction. In addition to the experimental works (Ishikura et al., 2003; He et al. 1994a, b) numerical simulation has evolved into a useful tool to obtain detailed information of flow phenomena in spouted beds. Little effort about Eulerian-Eulerian simulation of

spouted bed with a non-porous draft tube has been reported in the literature (Szafran and Kmiec, 2004). Zhao et al. (2008) has been simulated a two-dimensional spouted bed with draft plates using a combined technique of discrete element method and fluid dynamic computation (DEM-CFD) considering the gas turbulence effect.

In the present study, a 2D turbulent multi-fluid model based on the kinetic theory of granular flow is used for simulation of spouted bed with a non-porous draft tube, in which binary mixture of particles are contained. The frictional constitutive model is used for the solid phase. Hydrodynamic parameters are investigated at different operating situations. Furthermore, entrainment height and draft tube diameters as geometry parameters are studied.

MODEL DESCRIPTION

Multi-fluid Eulerian–Eulerian model is used. In this model, all phases are mathematically treated as interpenetrating continua. The success of multi-fluid model (MFM) depends on proper description of the interfacial forces and the solid stresses. The interfacial forces are used to describe the momentum transfer between the phases, which has the primary effect on the hydrodynamic behaviour. The solid stress, which represents the solid phase forces due to the particle–particle collisions, has an important effect in dense flows. By introducing the concepts of solid pressure and solid viscosity, the well established granular kinetic theory has been employed for computation of the solid stress.

Governing equations

The continuity and momentum equations for the gas and solid phases in the multi-fluid model in the absence of growth, aggregation and breakage phenomena are:

Continuity for phase k ($k = g$ for gas or m for solids):

$$\frac{\partial}{\partial t}(\alpha_k \rho_k) + \frac{\partial}{\partial x_i}(\alpha_k \rho_k u_{ki}) = 0 \quad (1)$$

Momentum equations for solids phases $m = 1, M$:

$$\left[\frac{\partial}{\partial t}(\alpha_m \rho_m u_{mi}) + \frac{\partial}{\partial x_j}(\alpha_m \rho_m u_{mj} u_{mi}) \right] =$$

$$-\alpha_m \frac{\partial P_g}{\partial x_i} + \frac{\partial \tau_{mij}}{\partial x_j} + I_{gmi} - \sum_{n=1}^M I_{kni} + \alpha_m \rho_m g_i \quad (3)$$

Momentum equations for gas phase g :

$$\left[\frac{\partial}{\partial t}(\alpha_g \rho_g u_{gi}) + \frac{\partial}{\partial x_j}(\alpha_g \rho_g u_{gj} u_{gi}) \right] =$$

$$-\alpha_g \frac{\partial P_g}{\partial x_i} + \frac{\partial \tau_{gij}}{\partial x_j} - \sum_{n=1}^M I_{gmi} + \alpha_g \rho_g g_i \quad (4)$$

where α_g and α_m are the volume fractions for the gas and solid phases. The sum of the volume fractions of all phases is unity. u_g and u_m are velocity vectors of the gas and solid phases, respectively.

Granular temperature equations for solids phases $m = 1, M$:

$$\frac{3}{2} \alpha_m \rho_m \left[\frac{\partial \Theta_m}{\partial t} + u_{mj} \frac{\partial \Theta_m}{\partial x_j} \right] = \frac{\partial}{\partial x_i} \left(\alpha_m \rho_m \kappa_m \frac{\partial \Theta_m}{\partial x_i} \right) + \alpha_m \rho_m \tau_{mij} \frac{\partial u_{mi}}{\partial x_j} + \Pi_m - \alpha_m \rho_m J_m \quad (5)$$

In equation (4) gas/solids momentum interface exchange is:

$$I_{gmi} = \beta_{gm} (u_{gi} - u_{mi}) \quad (6)$$

where β_{gm} describes drag coefficient. The Wen and Yu drag model is used in present study:

$$\beta_{gm} = \frac{3}{4} C_D \frac{\rho_g \alpha_g \alpha_m}{d_{p,m}} |\mathbf{u}_g - \mathbf{u}_m| \alpha_g^{-2.65} \quad (7)$$

where the drag coefficient, C_D , is:

$$C_D = \begin{cases} \frac{24}{\alpha_g \text{Re}} [1 + 0.15(\alpha_g \text{Re})^{0.687}], & \text{Re} < 1000 \\ 0.44 & , \text{Re} \geq 1000 \end{cases} \quad (8)$$

where $\text{Re} = \frac{\rho_g |\mathbf{u}_g - \mathbf{u}_m| d_{p,m}}{\mu_g}$

Solids/solids momentum exchange is expressed as:

$$I_{kmi} = -\beta_{km} (u_{ki} - u_{mi}) \quad (9)$$

and

$$\beta_{km} = \frac{3(1+e)(\pi/2 + C_{fkm} \pi^2/8) \alpha_k \rho_k \alpha_m \rho_m (d_{p,m} + d_{p,k})^2}{2\pi(\rho_m d_{p,m}^3 + \rho_k d_{p,k}^3)} \times g_{0,mk} |\mathbf{u}_m - \mathbf{u}_k| \quad (10)$$

e and C_{fkm} are coefficients of restitution and friction between the solids-phases. The radial distribution function, $g_{0,mk}$ for a mixture of hard spheres was expressed as:

$$g_{0,mk} = \frac{1}{\alpha_g} + \frac{3d_{p,m} d_{p,k}}{\alpha_g^2 (d_{p,m} + d_{p,k})} \sum_{n=1}^M \frac{\alpha_n}{d_{p,n}} \quad (11)$$

Solid phase stress tensor is shown as follows:

$$\tau_{mij} = \left(-P_m + \eta \mu_b \frac{\partial u_{mi}}{\partial x_i} \right) \delta_{ij} + 2\mu_m S_{mij} \quad (12)$$

where

$$S_{mij} = \frac{1}{2} \left(\frac{\partial u_{mi}}{\partial x_j} + \frac{\partial u_{mj}}{\partial x_i} \right) - \frac{1}{3} \frac{\partial u_{mi}}{\partial x_i} \quad (13)$$

Kinetic theory model are used for solid properties as follows:

Solids pressure:

$$P_m = \alpha_m \rho_m \Theta_m \left[1 + 4\eta \sum_{n=1}^M (\alpha_n g_{0,mn}) \right] \quad (14)$$

Solids viscosity:

$$\mu_m = \left(\frac{2+\alpha}{3} \right) \left[\frac{\mu_m^*}{g_{0,mm} \eta (2-\eta)} \left(1 + \frac{8}{5} \eta \sum_{n=1}^M (\alpha_n g_{0,mm}) \right) \times \left(1 + \frac{8}{5} \eta (3\eta-2) \sum_{n=1}^M (\alpha_n g_{0,mm}) \right) + \frac{3}{5} \eta \mu_b \right] \quad (15)$$

$$\mu_m^* = \frac{\rho_m \alpha_m g_{0,mm} \Theta_m \mu}{\rho_m \sum_{n=1}^M (\alpha_n g_{0,mm}) \Theta_m + \left(\frac{2\beta_{gm} \mu}{\rho_m \alpha_m} \right)} \quad (16)$$

$$\mu = \frac{5}{96} \rho_m d_p \sqrt{\pi \Theta_m}, \quad \mu_b = \frac{256}{5\pi} \mu \alpha_m \sum_{n=1}^M (\alpha_n g_{0,mm}) \quad (17)$$

Solids conductivity:

$$\kappa_m = \left(\frac{\kappa^*}{g_{0,mm}} \right) \times \left[\left(1 + \frac{12}{5} \eta \sum_{n=1}^M (\alpha_n g_{0,mm}) \right) \left(1 + \frac{12}{5} \eta^2 (4\eta-3) \sum_{n=1}^M (\alpha_n g_{0,mm}) \right) + \frac{64}{25\pi} (41-33\eta) \eta^2 \left(\sum_{n=1}^M (\alpha_n g_{0,mm}) \right)^2 \right] \quad (18)$$

$$\kappa^* = \frac{\kappa_0}{1 + \frac{6\beta_{gm} \kappa_0}{5(\rho_m \alpha_m)^2 g_{0,mm} \Theta_m}}, \quad \kappa_0 = \frac{75 \rho_m d_p \sqrt{\pi \Theta_m}}{48\eta(41-33\eta)} \quad (19)$$

Collisional dissipation:

$$J_m = \frac{48}{\sqrt{\pi}} \eta (1-\eta) \frac{\sum_{n=1}^M (\alpha_n g_{0,mm})}{d_p} \Theta_m^{\frac{3}{2}}, \quad \eta = \frac{1+e}{2} \quad (20)$$

Exchange terms:

$$\Pi_m = -3\beta_{gm} \Theta_m + \frac{81 \alpha_m \mu_g^2 |\mathbf{u}_g - \mathbf{u}_m|^2}{g_{0,mm} d_p^3 \rho_m \sqrt{\pi \Theta_m}} \quad (21)$$

The Srivastava and Sundaresan frictional model and $k-\varepsilon$ turbulent model are used for the solid and gas phases, respectively. More details about these models are found in Reference (Benyahia et al., 2006).

Model solution procedure

In this study, the experimental results of Ishikura et al. (2003) in a spouted bed containing non-porous draft tube with the parameters indicated in Tables 1 and 2 were adopted to validate the model predictions. The gas was air and the solids were glass beads. CFD code MFIX, was used to simulate the hydrodynamics of a spouted bed with a non-porous draft tube. The system is assumed to be axially symmetry. The set of governing equations are solved by a finite control volume technique. SIMPLE algorithm is utilized. A convergence criterion of 10^{-3} for each scaled residual component is fixed for the relative error between two iterations. The boundary conditions are as follow:

1. At the bottom of the bed, the gas injects only in the axial direction, so the inlet gas velocity is used as: $u_{x,0} = 0$ and $u_{y,0} = 69.44 \text{ U}$
2. The pressure boundary condition is set at atmospheric on the top of the freeboard.
3. On the bed wall, a no slip and on the internal and external wall of the tube, free slip boundary conditions are assumed.
4. In Current study, the axis is initialized as a free-slip wall.

Computational domain	Unit	Value
Diameter of column	m	0.10
Height of column	m	1
Diameter of nozzle	m	0.012
Cone angle	degree	60
Tube inside diameter	m	0.014, 0.018
Tube length	m	0.3
Distance of tube from nuzzle	m	0.02, 0.03, 0.04
Initial static bed height from nuzzle	m	0.3

Table 1: CFD domain scales.

RESULTS

The coefficient of restitution is a measure of the elasticity of the collision between two particles. It ranges between perfectly inelastic ($e = 0$) and perfectly elastic ($e = 1.0$). The coefficient of restitution affects the momentum and granular conservations of the solid phase. Since the particle diameters in spouted bed are usually larger than 1 mm and particle velocities in annulus region are low, so these systems should have low value of coefficient of restitution. Simulations are carried out for restitution coefficient of 0.8, 0.85, 0.9, 0.95, and 0.99. It is observed that a restitution coefficient of 0.85 give reasonably good predictions.

Particle properties	Unit	Operational conditions
Number of solid phase, N	–	2
Diameters, d_{pm}	μm	477, 1351
Mass fraction of finer particles	kg/kg	0.0, 0.05, 0.15, 0.5, 1.0
Density, ρ_{ms}	kg/m ³	2480
Coefficient of restitution, e	–	0.85
angle of internal friction	degree	28.5
Initial value of void fraction, α_{mf}	–	0.37–0.39
Gas property	–	–
Density, ρ_g	kg/m ³	1.2
Viscosity, μ_g	Pa·s	1.8×10^{-5}

Table 2: Gas and particles properties.

One of the dominant forces in fluidized beds is drag force. In this study, different drag models of Gibilaro, Zhang-Reese, Syamlal-O'Brien, Gidaspow, and Wen-Yu are examined. It is found that the drag model of Wen-Yu is the best choice for the spouted bed with a non-porous draft tube and has been used in the rest of the simulations.

Solid velocity vector

Fig. 1 show the predicted results of particle velocity vector in the whole bed. By considering particle flow pattern in conventional spouted bed, the flow pattern of particles in a spouted bed with draft tube is relatively

regular. Particles are first entrained from the bottom of the draft tube. Then they move upward within the draft tube under the drag force of fluids, rise into the fountain, fall down in the annulus, and finally they move slowly in the annulus for the next entrainment. The magnitude of solid particle velocity is high in the spout region with a maximum value of 2.28 m/s, indicating dilute flow, while the magnitude of particle velocity in the annulus is low, with a value of only 0.07 m/s, indicating a dense granular flow. Fig. 1 illustrates the distance of entrainment zone, H_D , which determines the flux of particle circulating from the annulus to the spout. This finding has been confirmed by Zhao et al. (2008). As a clear result, draft tube provides a means for suitable controlling particle history. The model is suitable for predicting the solid velocity vector but not for each type of particles.

Gas flow rate through the annulus and cone regions

Fig. 2a shows the relationship between the gas flow rate through the annulus ($Q_A/Q_T = V_A \cdot A_A / V_T \cdot A_T$) and different vertical distance y from the gas inlet nozzle in annular radius of 0.015 m for two sets, one is $C_S = 0.0$ (C_S is ratio of mass of finer particles divided by mass of whole bed) while $U = 0.414$ m/s, the second is $C_S = 0.05$ while $U = 0.362$ m/s. It is worth to mention that experimental data for the cone section have not been reported in the literature. Good agreement is obtained between the simulation and the experimental results in annulus region for both binary mixture and mono-size particles. The simulation result shows that the Q_A/Q_T increases almost exponentially with y and reaches a constant value at $y = 10$ cm. On the other hand, the Q_A/Q_T profile becomes flat along the tube because of lacking radial gas percolation within the non-porous draft tube. To investigate the effect of C_S on Q_A/Q_T through annulus region, three mass fraction of finer particles of 0.05, 0.15 and 0.5 at $U = 0.298$ m/s are simulated (Fig. 2b). Predicted result shows that Q_A/Q_T decreases with increasing C_S .

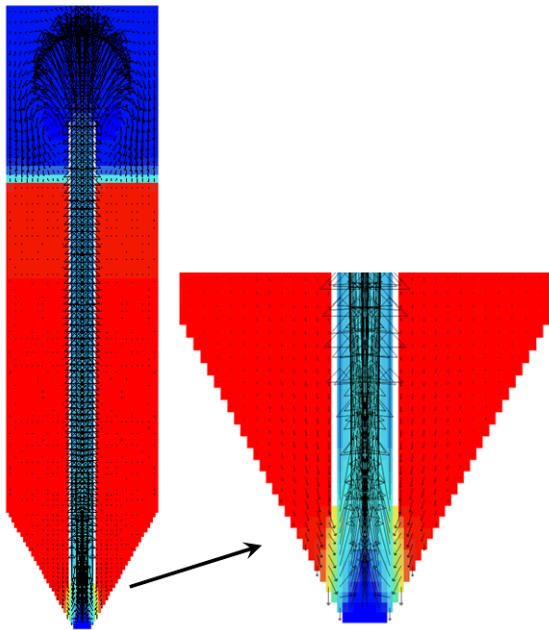


Fig. 1: Particle velocity vector in the whole bed
To investigate the gas flow rate through the annulus in porous draft tube, the spouted bed including porous draft tube also simulated using Gidaspow drag model and

Srivastava and Sundaresan frictional model. As can be seen in Fig. 3, unlike the non-porous draft tube, the porous draft tube indicates non-uniform distribution of gas flow rate in annulus because of gas percolation within the porous draft tube.

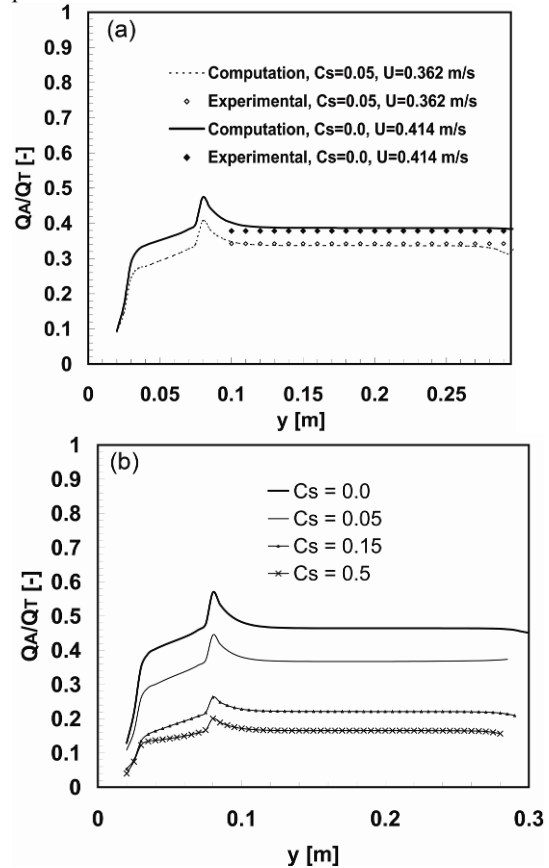


Fig. 2: Relationship between the gas flow rate through annulus and vertical distance as parameters of C_S in annular radius of 0.015m.

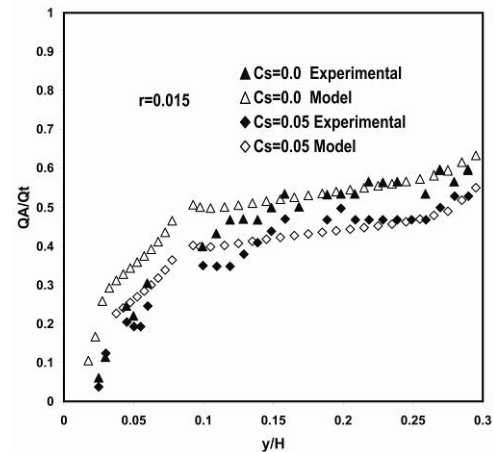


Fig. 3: The gas flow rate through annulus versus vertical distance as parameters of C_S in annular radius of 0.015m for the porous draft tube.

Gas flow pattern

Fig. 4a shows the contour plot of axial gas velocity in the annulus region of the bed for the case of $C_S = 0.05$ and $U = 0.362$ m/s. The experimental value of gas flow rate in annulus is 9.73×10^{-4} m³/s. The predicted value is 9.58×10^{-4} m³/s. Therefore the simulation and experimental data have a good agreement in term of axial gas velocity in

annulus region. It can be seen from the simulation that the gas velocity in spout region is 100 times higher than its corresponding value in annulus region. Fig. 4b indicates the gas velocity vectors in the bed.

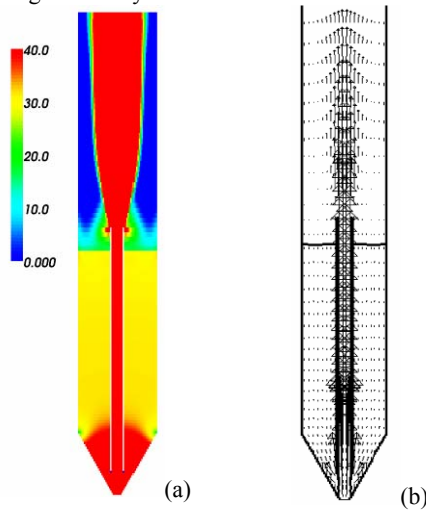


Fig. 4: Contour plot of axial gas velocity in annulus section and vector plot of gas velocity in spout and annulus regions.

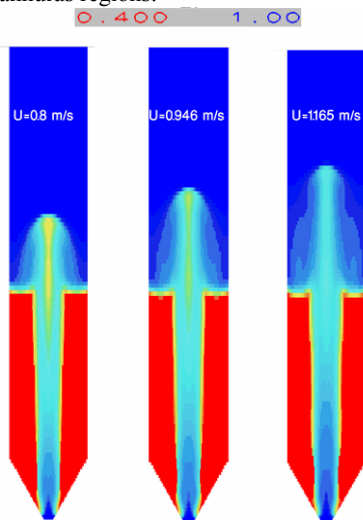


Fig. 5: Solid volume fraction at the increasing injected gas velocity.

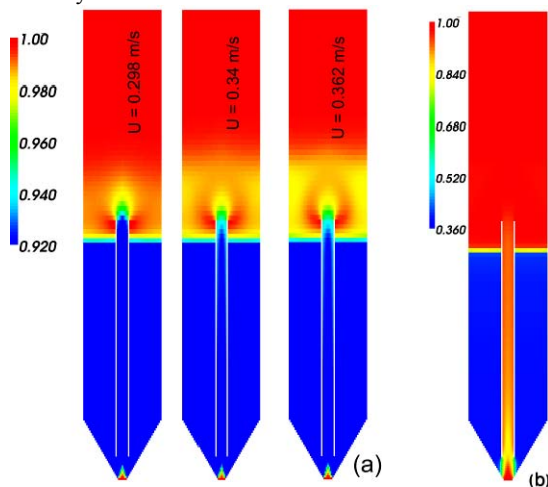


Fig. 6: gas volume fraction at the increasing injected gas velocity.

The gas phase first enters from the equipped nozzle in the bottom of the bed and then moves upward within both the draft tube and annulus section of the bed and finally exits from the top of the bed.

Fountain and spout region

The spouted bed without draft tube (conventional) is simulated at different injected gas velocities by applying switch function in Gidaspow's drag model. Fig. 5 describes the solid particle volume fraction distributions within the spouted bed, when the injected gas velocity is increased from 1.1 to 1.6 U_{ms} . The minimum spouting velocity, U_{ms} , was 0.73 m/s in Ishikura et al.'s experiments, for a static bed height of 0.30 m in ordinary spouted bed. In Fig. 5 a spouted bed is formed and its three characteristic regions i.e. the spout, the fountain and the annulus, are clearly observed. From Fig. 5, it is also observed that near the top of the spout and in the centre of the fountain, there exists a somewhat denser zone around the spout axis especially at lower gas velocities which were confirmed by researchers both experimentally (Grace and Mathur, 1978; He et al., 1994a,b) and numerically (Du et al., 2006a,b; Zhonghua and Mujumdar, 2008). This figure indicates that by increasing the gas velocity, the fountain height increases which is consistent with previous reports (He et al., 1994a,b; Du et al., 2006a,b; Zhonghua and Mujumdar, 2008; Olazar et al., 2001).

Fig. 6a describes the gas volume fraction at the range of 0.92 to 1.0 through spouted bed with draft tube. The injected gas velocity ranges from $U = 0.298$ to 0.362 m/s. In the post processing stage, the high range of gas volume fraction was selected to indicate the low value of solid concentration at fountain zone. According to Fig. 6a, when the gas velocity is increased, the fountain height increases. By considering Figs. 6a and 6b ($U = 0.362$ m/s), characteristic of the three regions i.e. the spout, the fountain and the annulus, can be clearly observed when the gas velocity is increased further. According to Figs. 5 and 6a, similarities between flow pattern with draft tube, and without draft tube, on the spouted bed are obtained. From Fig. 6a, it can also be seen that by increasing gas velocity, the particle circulation rate increases, because of growth of the solid concentration, which returns to the annulus region. This phenomenon has been confirmed by Ishikura et al. (2003).

Effects of U and C_S on superficial gas velocities of spout and annulus regions

Fig. 7 shows the effects of U and C_S on both the superficial gas velocity through annulus, U_A , and the superficial gas velocity within the draft tube or spout region, U_D . As it is shown in Figs. 7a, 7b and 7c, both U_A and U_D increase by increasing the superficial gas velocity, U . From this figure, it can be observed that the model predicts good results both in spout and in annulus regions of the bed. In addition, Fig. 7c clearly indicates that U_A decreases and U_D increases by increasing C_S . This is due to the drag force and cohesive forces between the particles. By increasing C_S the mean sauter diameter of particles reduces which leads to enhancement of drag force and particles velocity in the spout region. On the other hand decreasing the particles diameter causes increasing of cohesive forces between the solid particles in annulus region.

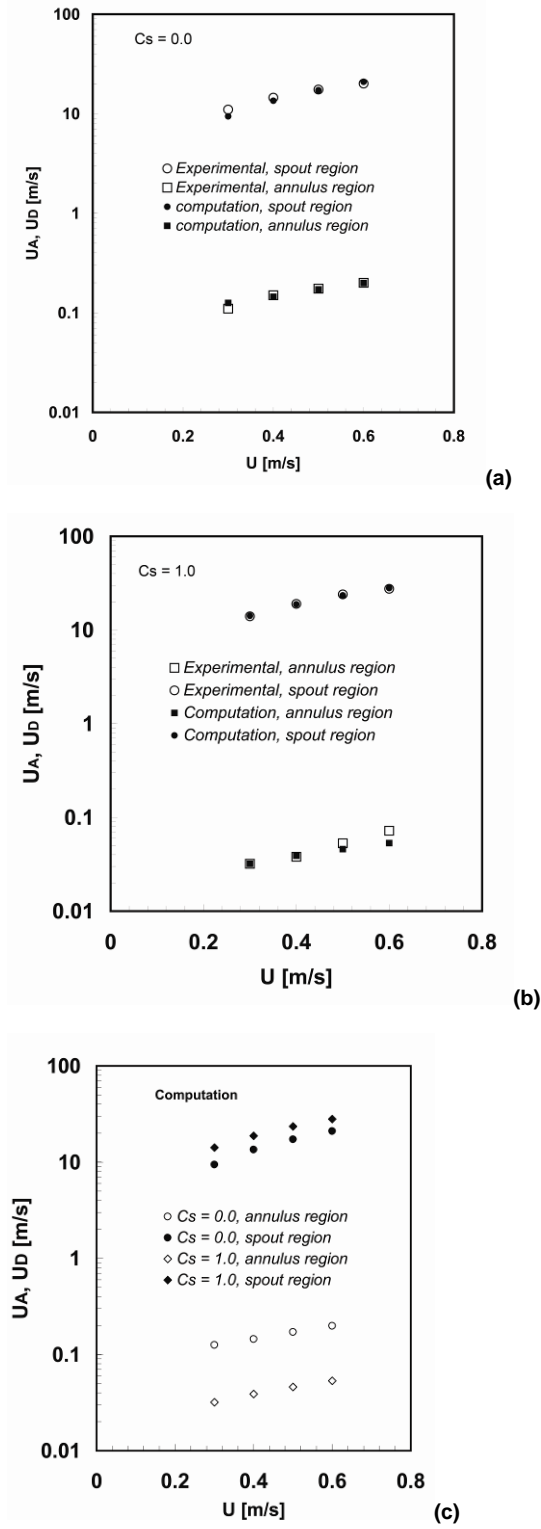


Fig. 7: Effect of U on gas velocity through annulus and draft tube with different C_s .

Effects of geometry parameters, H_D and D_D , on gas flow rate in annulus

Fig. 8 shows the effect of the geometry parameter H_D on gas flow rate within annulus for $C_s = 0.05$. As it is shown, Q_A/Q_T decreases with increasing Q_T and increases with increasing H_D for each system. This is due to the jet expansion. Simulation results show good agreement with experimental data, especially at low values of H_D . By

increasing H_D , the behaviour of the system is close to the conventional spouted bed. Better results can be obtained by changing parameters of the model such as restitution coefficient and drag model.

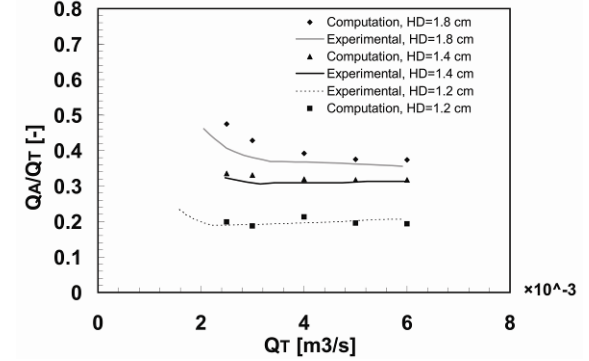


Fig. 8: Effect of H_D on Q_A/Q_T at different gas flow rate.

Fig. 9 shows the effect of non-porous draft tube diameter D_D on Q_A/Q_T for $C_s = 0.05$. This figure indicates that with increasing D_D , the Q_A/Q_T decreases. From Figs. 8 and 9, it can be concluded that the current model can also be used for the investigation of geometric parameters for scale-up and optimization processes in spouted bed with a non-porous draft tube.

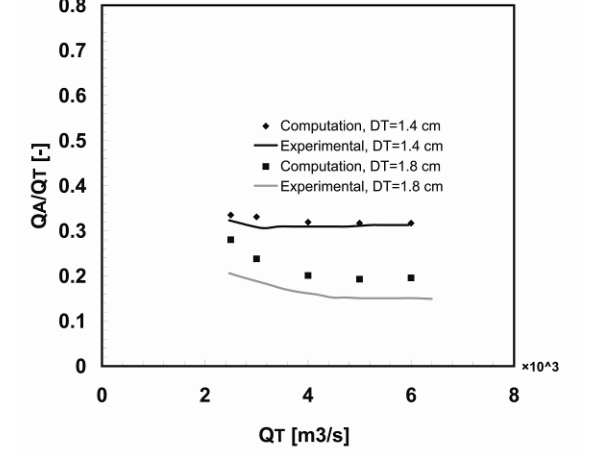


Fig. 9: Effect of D_D on Q_A/Q_T at different gas flow rate.

Pressure

By considering energy consumption of spouted bed systems, getting information of pressure is important. The longitudinal pressure distribution within annulus and spout region for a non-porous draft tube is shown in Fig. 10. It can be seen that pressure distribution through spout section is greater than annular part, especially in cone section of the bed.

CONCLUSION

Multi-Fluid Eulerian–Eulerian approach has been used for the simulation of spouted bed with a non-porous draft tube. This study can be used for understanding mechanism of gas–solid flow in the spouted bed with a non-porous draft tube. CFD results predict the flat profile of Q_A/Q_T along the bed in annulus region for the non-porous draft tube while non-uniform profile of Q_A/Q_T for porous draft tube. Predicted results illustrate three regions namely spout, fountain and annulus similar to conventional spouted bed. Effect of C_s on behaviour of the system was also investigated. By increasing the C_s , U_A decreases and U_D increases. The predicted results of longitudinal

pressure distribution are lower than experimental data, but these results show the same trends in spout and annulus regions. CFD results show that the model can predict hydrodynamic parameters of the spouted bed with a non-porous draft tube in annulus and spout regions reasonably well. The CFD tool can provide important information on the flow field within the spouted beds with a non-porous draft tube for design process, scale up, optimization and minimizing experimental efforts.

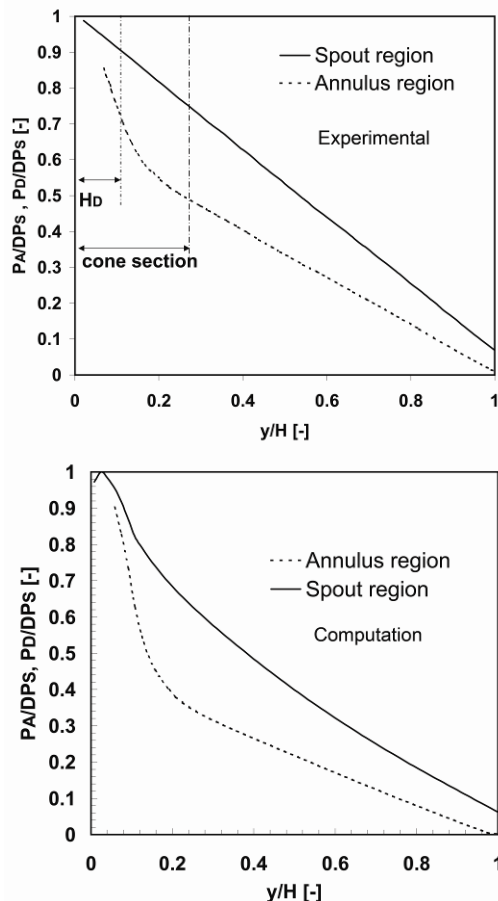


Fig. 10: Longitudinal pressure distribution within annulus and spout region for a non-porous draft tube spouted bed in annular radius of 0.015m.

REFERENCES

- ALTZIBAR, H., LOPEZ, G., ALVAREZ, S., SAN JOSÉ, M. J., BARONA, A. AND OLAZAR, M., (2008), "A draft-tube conical spouted bed for drying fine particles", *Dry. Technol.*, **26** (3), 308 – 314.
- BENYAHIA, S., SYAMLAL, M. AND O'BRIEN, T.J., (2006), "Summary of MFIx Equations 2005-4", From URL <http://www.mfix.org/documents/MfixEquations2005-4.pdf>.
- DU, W., BAO, X.J., XU, J. AND WEI, W.S., (2006a), "Computational fluid dynamics (CFD) modeling of spouted bed: assessment of drag coefficient correlations", *Chem. Eng. Sci.*, **61** (5), 1401-1420.
- DU, W., BAO, X.J., XU, J. AND WEI, W.S., (2006b), "Computational fluid dynamics (CFD) modeling of spouted bed: influence of frictional stress, maximum packing limit and restitution coefficient of particles", *Chem. Eng. Sci.*, **61** (14), 4558 – 4570.

FERREIRA, M. C. AND FREIRE, J. T., (1992), "Fluid dynamics characterization of a pneumatic bed using a spouted bed type solid feeding system", *Can. J. Chem. Eng.*, **70** (5), 905-909.

FUKUMORI, Y. AND ICHIKAWA, H., (1997), "Micro encapsulation of Pharmaceuticals by Fluidized Bed Process", *J. Soc. Powder Technol., Jpn.*, **34**, 536–544.

GRACE, J.R. AND MATHUR, K.B., (1978), "Height and structure of the fountain region above spouted beds", *Can. J. of Chem. Eng.*, **56**, 533–537.

HATATE, Y., MIHARA, H., IJICHI, K., YOSHIMI, T., ARIMIZU, S., UEMURA, Y. AND KING, D.F., (1996), "Catalytic Coal Gasification Using a Draft Tube Spouted Bed Gasifier", *Kagaku Kogaku Ronbunshu*, **22**, 1180–1184.

HATATE, Y., IJICHI, K. AND UEMURA, Y., (1997), *J. Soc. POWDER TECHNOL., JPN.*, **34**, 343– 360.

HE, Y.L., LIM, C.J., GRACE, J.R., ZHU, J.X. AND QIN S.Z., (1994a), "Measurements of voidage profiles in spouted beds", *Can. J. Chem. Eng.*, **72**, 229–234.

HE, Y.L., LIM, C.J. AND GRACE, J.R., (1994b), "Particle velocity profiles and solid flow patterns in spouted beds", *Can. J. Chem. Eng.*, **72**, 561–568.

ISHIKURA, T., NAGASHIMA, H., IDE, M., (2003), "Hydrodynamics of a spouted bed with a Porous draft tube containing a small wall amount of finer particles", *Powder Technol.*, **131**, 56–65.

KHOE, G. K. AND VAN BRAKEL, J., (1983), "Drying characteristics of a draft tube spouted bed", *Can. J. Chem. Eng.*, **61**, 411 –418.

KONDURI, R. K., ALTWICKER, E. R. AND MORGAN III, M. H., (1995), "Atmospheric spouted bed combustion: The role of hydrodynamics in emissions generation and control", *Can. J. Chem. Eng.*, **73** (5), 744–754.

KRAMBROCK, W., (1976), "Mixing and homogenizing of granular bulk material in a pneumatic mixer unit", *Powder Technol.*, **15**, 199–206.

OLAZAR, M., SAN JOSÉ, M. J., IZQUIERDO, M.A., DE SALAZAR, A.O. AND BILBAO, J., (2001), "Effect of operating conditions on solid velocity in the spout, annulus and fountain of spouted beds", *Chem. Eng. Sci.*, **56** (11), 3585-3594.

STOCKER, R.K., ENG, J.H., SVRCEK, W.Y. AND BEHIE, L.A., (1989), "Ultraprolysis of propane in a spouted-bed reactor with a draft tube", *AIChE J.*, **35**, 1617–1624.

SZAFRAN, R.G. AND KMIEC, A., (2004), "CFD Modeling of Heat and Mass Transfer in a Spouted Bed Dryer", *Ind. Eng. Chem. Res.*, **43**, 1113–1124.

ZHAO, X.-L., LI, S.-Q., LIU, G.-Q., SONG, Q. AND YAO Q., (2008), "Flow patterns of solids in a two-dimensional spouted bed with draft plates: PIV measurement and DEM simulations", *Powder Technol.*, **183**, 79–87.

ZHONGHUA, W. AND MUJUMDAR, A.S., (2008), "CFD modeling of the gas-particle flow behavior in spouted beds", *Powder Technol.*, **183**, 260–272.